

OPEN ACCESS

## Competing Ethylene Carbonate Reactions on Carbon Electrode in Li-Ion Batteries

To cite this article: Robin Lundström *et al* 2023 *J. Electrochem. Soc.* **170** 040516

View the [article online](#) for updates and enhancements.

### You may also like

- [Benefits of Fast Battery Formation in a Model System](#)  
Peter M. Attia, Stephen J. Harris and William C. Chueh
- [Origin of H<sub>2</sub> Evolution in LIBs: H<sub>2</sub>O Reduction vs. Electrolyte Oxidation](#)  
Michael Metzger, Benjamin Strehle, Sophie Solchenbach et al.
- [DFT Study of Reduction Mechanisms of Ethylene Carbonate and Fluoroethylene Carbonate on Li<sup>+</sup>-Adsorbed Si Clusters](#)  
Yuguang Ma and Perla B. Balbuena

**Investigate your battery materials under defined force!**  
**The new PAT-Cell-Force, especially suitable for solid-state electrolytes!**



- Battery test cell for force adjustment and measurement, 0 to 1500 Newton (0-5.9 MPa at 18mm electrode diameter)
- Additional monitoring of gas pressure and temperature


[www.el-cell.com](http://www.el-cell.com) +49 (0) 40 79012 737 [sales@el-cell.com](mailto:sales@el-cell.com)

**EL-CELL®**  
electrochemical test equipment





# Competing Ethylene Carbonate Reactions on Carbon Electrode in Li-Ion Batteries

Robin Lundström,<sup>z</sup> Neeha Gogoi,<sup>ib</sup> Xu Hou,<sup>ib</sup> and Erik J. Berg<sup>z</sup> 

Department of Chemistry, Ångström Laboratory, Uppsala University, SE-751 21 Uppsala, Sweden

Ethylene carbonate (EC) is the archetype solvent in Li-ion batteries. Still, questions remain regarding the numerous possible reaction pathways of EC. Although the reaction pathway involving direct EC reduction and SEI formation is most commonly discussed, EC ring-opening is often observed, but seldomly addressed, especially with respect to SEI formation. By applying Online Electrochemical Mass Spectrometry, the EC ring-opening reaction on carbon is found to start already at ~2.5 V vs Li<sup>+</sup>/Li as initiated by oxygenic carbon surface groups. Later, OH<sup>−</sup> generated from H<sub>2</sub>O reduction reaction at ~1.6 V further propagates EC to ring-open. The EC reduction reaction occurs <0.9 V but is suppressed depending on the extent of EC ring-opening at higher potentials. Electrode/electrolyte impurities and handling conditions are found to have a significant influence on both processes. In conclusion, SEI formation is shown to be governed by several kinetically competing reaction pathways whereby EC ring-opening can play a significant role.

© 2023 The Author(s). Published on behalf of The Electrochemical Society by IOP Publishing Limited. This is an open access article distributed under the terms of the Creative Commons Attribution 4.0 License (CC BY, <http://creativecommons.org/licenses/by/4.0/>), which permits unrestricted reuse of the work in any medium, provided the original work is properly cited. [DOI: 10.1149/1945-7111/acb6e]



Manuscript submitted January 20, 2023; revised manuscript received March 7, 2023. Published April 18, 2023. The majority of the data was presented at the 239th ECS Digital Meeting in presentation A02-0147, May 30-June 3, 2021

Supplementary material for this article is available [online](#)

Fossil based energy is getting phased out in favor of renewable energy.<sup>1</sup> Improved energy solutions are however needed to accelerate the progress where Li-ion batteries (LIBs) play a central role as the highest performing energy storage technology on the market. Still, several challenges remain and impede further implementation of battery energy storage applications. For instance, LIBs experience continuous energy loss over time, their electric impedances increase and fractions of capacities are lost in every charge-discharge cycle.<sup>2</sup> The processes can partly be traced back to the negative graphite electrode and its interface towards the electrolyte in the Li-ion cell. The highly reducing environment at the negative electrode leads to the formation of a passivation layer, called Solid Electrolyte Interphase (SEI), separating the electrode surface from the electrolyte. The function of the SEI is to prevent further breakdown of electrolyte and, at the same time, remain conductive for Li<sup>+</sup> to maintain the operation of the graphite electrode.<sup>2,3</sup> The performance of the SEI is well-recognized in the field to be critical for the LIB cell, even though a final consensus on the composition, structure, formation and operating mechanism remains to be established. Our understanding of the SEI in LIBs has gradually improved over the past few decades. Peled presented the first model in 1979, which claimed that alkali metals, in contact with electrolyte, are always covered by an electronically insulating surface layer.<sup>4</sup> The electronically insulating SEI was later confirmed to form on carbon surfaces as well,<sup>5</sup> but SEI formation reactions and resulting products are defined by both electrode surface and electrolyte composition.

Ethylene carbonate (EC) is the main Li-ion electrolyte solvent as well as the archetype SEI former in Li-ion cells. A compelling map reviewing possible EC reaction pathways was presented and validated with kinetic Monte Carlo simulations by Spotte-Smith et al., that again showcased the complexity of EC reactions during the SEI formation.<sup>6</sup> The foremost anticipated reaction of EC is its electrochemical reduction at ~0.8 V vs Li<sup>+</sup>/Li on carbon anode during cell formation (Fig. 1, Reactions I-IV), herein named “EC reduction.” Most commonly observed products are lithium carbonate (Li<sub>2</sub>CO<sub>3</sub>), lithium ethylene di-carbonate (Li<sub>2</sub>C<sub>4</sub>O<sub>6</sub>H<sub>4</sub>, abbr. LEDC), and ethylene (C<sub>2</sub>H<sub>4</sub>). Both Li<sub>2</sub>CO<sub>3</sub> and LEDC are insoluble in the electrolyte and precipitate on the electrode surface to form the SEI.<sup>7,8</sup>

EC is however susceptible to other side-reactions as well. Thermally activated ring-opening reactions (Fig. 1, reactions 1–4) are commonly observed, but seldomly discussed with regards to SEI formation. “EC ring-opening” is principally initiated by a nucleophilic attack on the EC ethylene carbon by a nearby Lewis base, e.g. as formed reductively at the negatively charged carbon electrode. Both hydroxides and alkoxides (Fig. 1, reactions 1a and b) have previously been observed to initiate the ring-opening of EC,<sup>11,12</sup> which in turn likely results in lithium ethyl carbonate (LiC<sub>3</sub>O<sub>4</sub>H<sub>5</sub>, abbr. LEMC) as an intermediate product. LEMC may further decompose into ethylene glycol (EG) and CO<sub>2</sub> (Fig. 1, reaction 2), both of which have been previously observed.<sup>11,13</sup> For instance, Metzger et al. linked EC ring-opening reaction to residual H<sub>2</sub>O (>40 °C) and OH<sup>−</sup> along with subsequent EC polymerization.<sup>11</sup> We hypothesize herein that the EC ring-opening reaction not only stems from H<sub>2</sub>O and OH<sup>−</sup>, but from other initiators as well, such as reduced oxygen<sup>14,15</sup> or oxygenic surface groups on the negative electrode (−OR<sup>−</sup>, Fig. 1, reaction 1a).

In principle, both EC reduction and EC ring-opening reactions can result in similar SEI products—inorganic and organic carbonates, hence rendering the two different types of reactions difficult to separate based on SEI composition only. However, the reactions can be distinguished by analyzing the evolving gases, where C<sub>2</sub>H<sub>4</sub> originates from EC reduction (Fig. 1, reactions II and IV) and CO<sub>2</sub> originates from EC ring-opening reactions (Fig. 1, reactions 2 and 3). In addition, EC ring-opening can occur at higher potentials compared to the EC reduction reactions.

In practice, Li-ion cell formation is typically conducted under galvanostatic conditions predominantly triggering the reduction of EC or other layer-forming additives. EC ring-opening reactions do however occur in parallel and may prevail as a homogeneous reaction in the electrolyte phase depending on the concentration of remaining ring-opening initiators. This continuous reaction is easily overlooked since the resulting CO<sub>2</sub> evolution also trigger CO<sub>2</sub> consumption reactions <1.5 V, which in turn thickens the SEI.<sup>16</sup> In any case, the CO<sub>2</sub> evolution is seen if its evolution rate overtakes its consumption rate. The extent EC ring-opening reactions influence the SEI and the accompanied gassing processes in LIBs are not completely understood.

Numerous parallel processes will take place during the formation cycles in a LIB. Consequently, separating and studying a single or a few specific reactions with minimal influence from the rest of the LIB reactions is challenging. By using a relatively inert electrode

<sup>z</sup>E-mail: [robin.lundstrom@kemi.uu.se](mailto:robin.lundstrom@kemi.uu.se); [erik.berg@kemi.uu.se](mailto:erik.berg@kemi.uu.se)

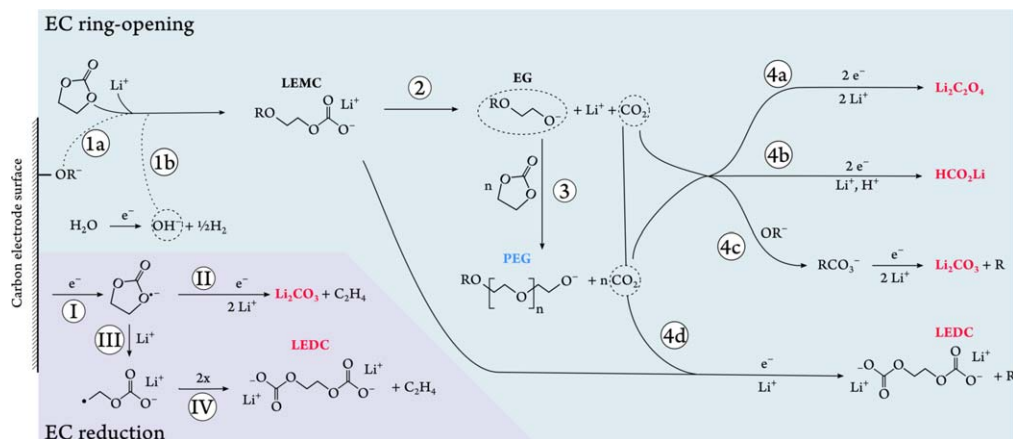


**Figure 1.** Suggested reaction pathways for EC ring-opening reaction (number reactions) and (direct) EC reduction (numeral reactions) on the carbon electrode surface. Species marked in red precipitate as SEI on the carbon electrode surface. Species marked in blue dissolve into the electrolyte. Circled species are intermediate products that continue to follow different reaction pathways. Reactants with dashed lines represent a choice where either species with a dashed line partake in the reaction. Only reactions relevant for this work are presented here for clarity. Numerous other reaction pathways are possible as well.<sup>2,9,10</sup>

material for the negative electrode, such as glassy carbon (GC), a few highly influential processes can be suppressed (such as solvent co-intercalation and electrode swelling). As a result, the studied EC reaction pathways can be highlighted.

The hypothesis of the study is that there is a competition between EC reduction and EC ring-opening reactions in contributing to SEI formation. Apart from validation, we aim to identify new possible reaction initiators, highlight experimental conditions affecting EC reactions, and further verify SEI formation products on carbon and in the electrolyte.

## Experimental

**Material and cell preparation.**—All cells were assembled the same way—an electrode sandwich consisting of GC | 1 M LiPF<sub>6</sub> EC:DEC | LiFePO<sub>4</sub> (LFP), where GC was always on top facing the gas headspace of the Online Electrochemical Mass Spectrometry (OEMS) cell.<sup>17</sup> The GC electrodes were prepared as a slurry consisting of 95 w% GC powder (Sigma-Aldrich, spherical powder, 2–12 μm, 99.95% trace metals basis, A<sub>BET</sub> = 1.8 m<sup>2</sup> g<sup>-1</sup>) and 5 w% PVDF (Kynar HSV 900, Arkema) dissolved in NMP solvent. The slurry was mixed for 30 min at 25 Hz (MM 400, Retsch) before coated on a stainless-steel mesh (212/90 μm, Bopp AG, Switzerland), using a doctor blade with a gap size of 150 μm. Electrodes were first dried at room temperature, before punched into 14 mm disks and dried at 120 °C under vacuum for 12 h. Afterwards, the GC electrodes were stored in an inert Ar atmosphere until cell assembly. The commercial LFP electrodes (1 or 2 mAh cm<sup>-2</sup>, Customcells) were punched into 15 mm disks and dried at 120 °C under vacuum for 12 h. The LFP electrodes were electrochemically delithiated to reach a stable potential plateau before cycled with GC (see supporting information (SI) for procedure). The LFP potential is assumed to be stable at 3.43 V vs Li<sup>+</sup>/Li throughout this study, and all data will be presented vs Li<sup>+</sup>/Li redox potential. All cells used 1 M LiPF<sub>6</sub> EC:DEC 1:1 volume ratio electrolyte (Solvionic) in the range 50–400 μl, and a single 16 mm Celgard 2325 separator (dried for 6 h at 70 °C in vacuum).

**Online electrochemical mass spectrometry (OEMS).**—Gas analysis experiments were conducted on our earlier described custom OEMS system.<sup>17</sup> The gas composition in the cell headspace was probed every 10 min and subsequently refilled with Ar carrier gas (purity 99.9999%, Air Liquide). The mass spectrometer was calibrated with the following calibration gases; 2000 ppm H<sub>2</sub> and 4000 ppm CO<sub>2</sub> in Ar, 2000 ppm CH<sub>4</sub> and C<sub>2</sub>H<sub>4</sub> in Ar and 2000 ppm O<sub>2</sub> in Ar (Air Liquide). The gas cell was adapted for this study, where a stainless-steel puck was force-fitted into the polyether ether

ketone (PEEK) inset (See Fig. S1). The adapted cell kept the full electrolyte volume in close proximity to the electrodes. The electrolyte volumes used were 50, 100, 200 and 400 μl. All cells rested for 5 h at open circuit potential (OCP) before cycling. Next, the cells were swept with cyclic voltammetry (CV) at 20 mV s<sup>-1</sup> between 3.03–3.33 V to estimate electrochemically active surface area (see Fig. S2). Continuing, the cells were cycled using CV at 0.1 mV s<sup>-1</sup> scan rate down to 0.05 V and then back up to either 1.5 V or 1.7 V. The temperature was kept constant at 30 °C throughout the whole experiment. The gas cell was dried at 120 °C under vacuum for 12 h before any experiment.

**Nuclear magnetic resonance (NMR).**—For NMR, a JEOL (1H, 500 MHz) spectrometer was used, and chemical shifts were recorded in parts per million. Anhydrous dimethylsulfoxide (DMSO)-d<sub>6</sub> (99.9%) from VWR was used as a deuterated solvent. Fluorinated ethylene propylene (FEP) NMR tube liners (outer diameter: 5 mm, Wilmad-LabGlass) were filled up with 200 μl of DMSO-d<sub>6</sub>. The mouth of the FEP tube was closed with a poly(tetrafluoroethylene) (PTFE) plug. FEP NMR tube was then placed inside a glass NMR tube (inner diameter: 5 mm) containing 200 μl of sample solution. The glass NMR tube was again closed with a PTFE stopper. The sample preparation was done in inert Ar atmosphere where the H<sub>2</sub>O content was kept below 1 ppm. All spectra were processed and analyzed by MestReNova 6.0.2–5475 (Mestrelab research, Spain). Extracted electrolytes were subjected to the same electrochemical protocol as the OEMS experiments in the same gas cell. 400 μl 1 M LiPF<sub>6</sub> EC:DEC electrolyte was used during cycling.

## Results and Discussion

Figure 2 shows the current response and the evolution rates of the dominating gases H<sub>2</sub>, CO<sub>2</sub> and C<sub>2</sub>H<sub>4</sub> for three nominally identical GC | 1 M LiPF<sub>6</sub> EC:DEC (200 μl) | LFP cells. The first cell, “Baseline”, was assembled immediately after the electrode drying procedure (as described above). Then, the “Water contaminated” cell was intentionally contaminated with 300 ppm H<sub>2</sub>O and assembled directly after the Baseline cell experiment finished. Finally, before assembly of the “Delayed” cell, the GC electrode was stored in inert Ar atmosphere for two weeks after the drying and immediate introduction of the electrode into the Ar glovebox. The electrode was stored to investigate if GC surface composition changed and affected gas evolution over time. All current responses display similar profiles with only minor deviations at the vertex potential. The majority of electrode charge in the 1st cycle is reversible (83 ± 2%) and can be ascribed to Li<sup>+</sup> de-/adsorption at the GC surface.<sup>18,19</sup> Current peaks from irreversible electrochemical reactions are found

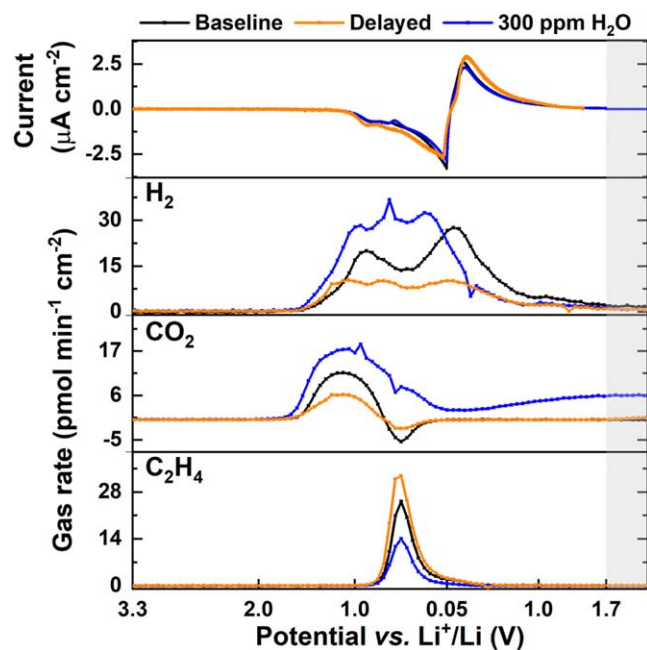


**Figure 2.** Current response and gas evolution rates for three nominally identical GC | 1 M LiPF<sub>6</sub> EC:DEC | LFP cells. The Delayed cell was intentionally delayed to store GC electrode in Ar atmosphere two weeks longer than the Baseline cell. The 300 ppm H<sub>2</sub>O was contaminated with water during cell assembly and followed directly after the Baseline cell. Greyed-out areas correspond to post-cycle OCP.

at 1.2 V and 0.84 V and partly relate to gas evolution reactions. The H<sub>2</sub> onset potentials and the shape of the evolution profiles for Baseline and Delayed cells are similar to the Water contaminated cell, which supports the notion that H<sub>2</sub> largely originates from water impurity reduction. Water is notoriously difficult to remove and even a nominally water-free commercial electrolyte (like the one employed herein) contains up to 20 ppm of H<sub>2</sub>O as determined from Karl-Fischer titration. According to Fig. 1, two H<sub>2</sub>O molecules are needed to generate a single H<sub>2</sub>. Hence, 20 and 300 ppm of water in 200  $\mu$ L electrolyte would correspond to 0.11 and 1.67  $\mu$ mol H<sub>2</sub>, respectively. These values represent 5%, 7%, and 60% of the total H<sub>2</sub> evolution for the Baseline (20 ppm H<sub>2</sub>O), Delayed (20 ppm H<sub>2</sub>O), and Water contaminated cells (300 ppm H<sub>2</sub>O), respectively. Any protic specie could however be reduced to evolve H<sub>2</sub>. Indeed, at least three H<sub>2</sub> evolution peaks are observed, possibly corresponding

to three distinct processes, of which only one would be immediately related to direct water reduction on GC. However, H<sub>2</sub> evolution could also be intermediately modulated by temporary passivation of the electrode surface during the SEI formation process, hence limiting surface access for H<sub>2</sub>O.<sup>20</sup> The exact reaction pathways for H<sub>2</sub> evolution in LIBs are not completely understood, but reduction of residual H<sub>2</sub>O and its subsequent reactions have mostly been proposed.<sup>21,22</sup> We do not assign any of the H<sub>2</sub> peaks to HF reduction since such a reaction and accompanied H<sub>2</sub> evolution proceeds >2 V (Fig. S3).

H<sub>2</sub> and CO<sub>2</sub> are correlated, and the gas evolution sets in at  $\sim$ 1.7 V regardless of the cell in Fig. 2. There are however clear differences in the evolution rates throughout the whole cycle. The Water contaminated cell shows that H<sub>2</sub>O reduction and formation of the Lewis base OH<sup>−</sup> increases the extent of H<sub>2</sub> and CO<sub>2</sub> evolution (Fig. 1, reactions 1b and 2). Furthermore, the Baseline cell evolves more H<sub>2</sub> and CO<sub>2</sub> than Delayed cell, indicating that the latter is subjected to change during inert storage in Ar.

Spahr et al. have previously shown that surface groups on carbon electrodes have a considerable effect on electrolyte reduction and SEI formation in LIBs.<sup>23,24</sup> Despite the vacuum and heat treatment of all electrodes, we hypothesize that the electrodes stored under Ar still continue to dry over time, losing physis- and chemisorbed water, and the oxygenic surface groups on carbon gradually disappear. Moreover, we hypothesize that the oxygenic surface groups can trigger EC ring-opening reaction (Fig. 1, Reaction 1a), as they are expected to be reduced before H<sub>2</sub>O reduction sets in.<sup>15,25</sup>

CO<sub>2</sub> evolution and consumption reactions occur in parallel and the high solubility of CO<sub>2</sub> in the organic carbonate-based electrolyte<sup>26,27</sup> complicate the determination of EC ring-opening onset potential in Fig. 2. First observation of CO<sub>2</sub> consumption is already at  $\sim$ 1.5 V, and likely induced by the formation of a significant number of Lewis bases (e.g. OH<sup>−</sup>) that in turn scavenge CO<sub>2</sub> (Fig. 1, reaction 4c). CO<sub>2</sub> consumption accelerates <1 V, possibly triggered by the reduction of EC setting in at the same time (Fig. 1, reaction I). Direct CO<sub>2</sub> reduction has been proposed as well, but reported to set in <0.7 V (Fig. 1, reactions 4a and 4b).<sup>16</sup> Even though EC reduction has been initiated at this stage, a fully impermeable SEI it not expected to form instantly.<sup>28,29</sup> CO<sub>2</sub> can get access to the GC surface by diffusing through the porous SEI. The Water contaminated cell shows CO<sub>2</sub> evolution during and after anodic sweep, which indicates that unreacted Lewis bases remain in the electrolyte (e.g. H<sub>2</sub>O, OH<sup>−</sup> or OR<sup>−</sup>).<sup>30</sup> Such a process is however only observed if the corresponding CO<sub>2</sub> evolution rates are higher than consumption rates. As a result, CO<sub>2</sub> evolution during the anodic sweep is detected at different potentials depending on the number of Lewis bases remaining.

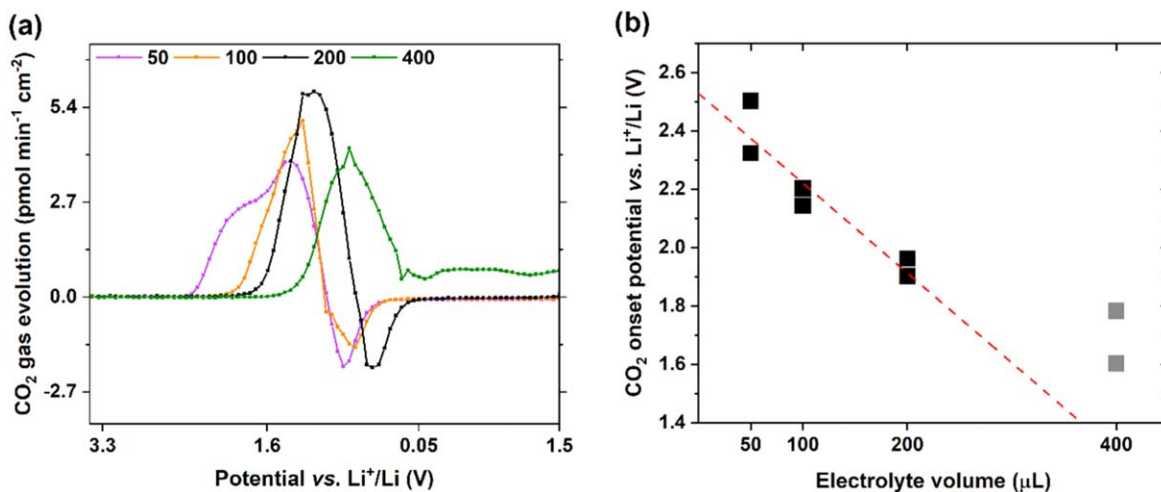


**Figure 3.** CO<sub>2</sub> gas evolution for different 1 M LiPF<sub>6</sub> EC:DEC electrolyte volumes. In (a)—The potential-dependent gas profiles. In (b)—The linear trend of CO<sub>2</sub> onset potential (400  $\mu$ L is excluded as other CO<sub>2</sub> evolving reactions have been initiated when CO<sub>2</sub> is first detected).



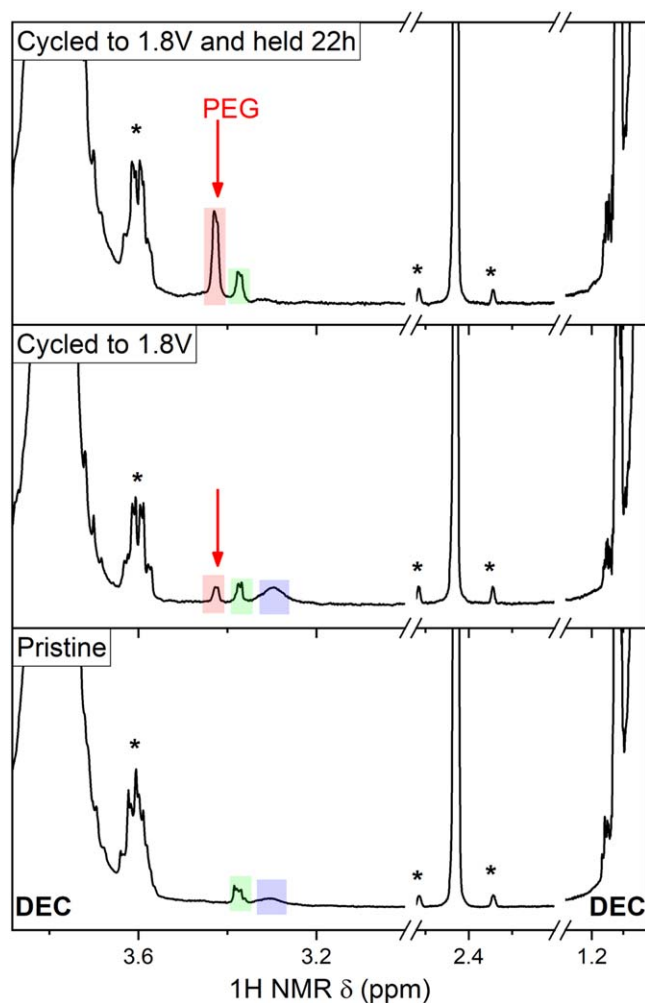


**Figure 4.**  $^1\text{H}$  NMR spectra of 1 M  $\text{LiPF}_6$  EC:DEC electrolyte (pristine, cycled to 1.8 V, cycled to 1.8 V and then potential held at 1.8 V for 22 h). The  $^{13}\text{C}$  satellites are marked with asterisks, and the new peaks (not EC/DEC) in the samples are shaded in red, green, and blue.

In order to investigate effects of  $\text{CO}_2$  solubility OEMS cells with different volumes of electrolyte were measured. Figure 3 shows that the onset potential of  $\text{CO}_2$  evolution shifts more positive the lower the available electrolyte volume in the cell. Even a linear trend for when  $\text{CO}_2$  evolution starts is found for cells with  $\leq 200\ \mu\text{l}$  electrolytes. Upon extrapolation, the true onset potential for EC ring-opening reaction of  $\sim 2.5\ \text{V}$  can be determined (Fig. 3b). This is the same potential range as when molecular oxygen is reduced (Fig. S4), which supports the notion that several oxygenic species, such as carbon surface groups, may trigger EC ring-opening as well. The  $400\ \mu\text{l}$  cell does not follow the same linear trend as the other cells, possibly because other  $\text{CO}_2$  evolving reactions are initiated before any  $\text{CO}_2$  is detected. Further evidence for a thermally activated EC ring-opening process is that no noticeable current was observed  $>1.6\ \text{V}$  in spite of a significant  $\text{CO}_2$  release. Other products of the ring-opening reaction, such as EG, continues to react with EC in solution, ultimately polymerizing into PEG and releasing more  $\text{CO}_2$  (Fig. 1, reaction 3).

Evidence for such a polymerization reaction pathway can be found by performing NMR Fig. 4 shows the  $^1\text{H}$  NMR spectra of extracted electrolyte examined at three different stages—1. Pristine electrolyte, 2. After cell was swept to 1.8 V, and 3. After cell was swept to 1.8 V and potential held at 1.8 V for 22 h. Strong signals arising from EC, DEC, and deuterated DMSO solvent are observed at 4.21 (EC,  $-\text{CH}_2-\text{CH}_2-$ ), 3.79 (DEC,  $-\text{CH}_2-$ ), 0.88 (DEC,

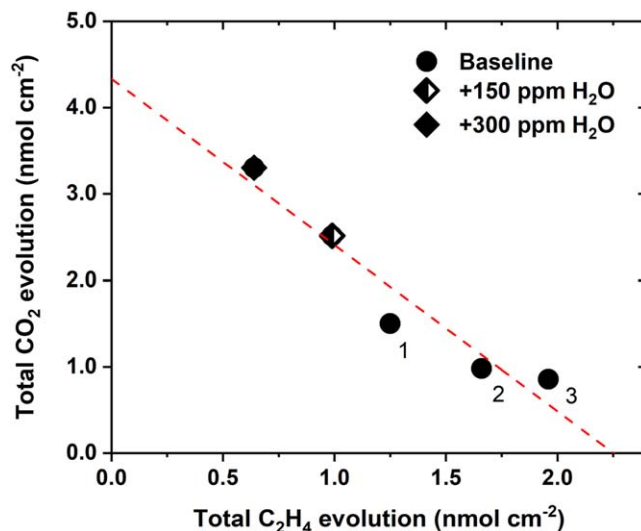


**Figure 5.** Linear trend for  $\text{CO}_2$  and  $\text{C}_2\text{H}_4$  evolution for GC | 1 M  $\text{LiPF}_6$  EC:DEC | LFP cells with pure electrolyte and with controlled addition of  $\text{H}_2\text{O}$  to the electrolyte. Numbering of the baseline cells indicates the order of assembly (higher number equals longer GC storage time in inert conditions after vacuum drying).

$-\text{CH}_3$ ), and 2.50 ppm (DMSO), respectively. Additionally, a signal at 3.37 ppm (shaded in green) is observed which is assigned to an electrolyte soluble impurity. This signal remains consistent in all the three samples indicating that this impurity does not reduce or react during the cycling of the cell, at least until 1.8 V. Moreover, a broad signal at 3.29 ppm is observed in the pristine electrolyte (shaded in blue), which is assigned to water present in the electrolyte in trace amount. The  $\text{H}_2\text{O}$  signal remains consistent in the electrolyte extracted from the cell that was cycled to 1.8 V. However, the signal nearly completely disappears for the electrolyte extracted from the cell that was cycled to 1.8 V and held for 22 h. This indicates that the  $\text{H}_2\text{O}$  is consumed during the potential hold, even though no  $\text{H}_2$  evolution is present in OEMS measurements with identical cycling protocol. A new peak (shaded in red) at 3.43 ppm appears in the electrolyte extracted from the cell that was cycled to 1.8 V, which grows for the electrolyte extracted from the cell that was held at 1.8 V for 22 h. This signal is assigned to PEG (Fig. 1, reaction 3). No quantitative analysis of PEG in the different samples were conducted, but an estimated PEG concentration would be in the range of 100 s of ppm after 22 h hold at 1.8 V. Only minor amounts of oxygenic surface groups are needed to propagate EC ring-opening,  $\text{CO}_2$  evolution and subsequent polymerization before  $\text{H}_2\text{O}$  reduction sets in. EC ring-opening reaction is therefore likely present in every LIB and impose a challenge unless controlled.

$\text{C}_2\text{H}_4$  gas evolution in Fig. 2 is observed  $<0.9\ \text{V}$  in all cells as a result of EC reduction, which is also anticipated to lead to the formation of  $\text{Li}_2\text{CO}_3$  and LEDC (Fig. 1, reactions II and IV). Both products are insoluble in the electrolyte and precipitate on the carbon surface to form the SEI. Interestingly, a larger volume of  $\text{C}_2\text{H}_4$  evolves for the Delayed cell compared to the Baseline, and lower volume of  $\text{C}_2\text{H}_4$  for the Water contaminated cell. Comparing the extents of  $\text{CO}_2$  evolution  $>1\ \text{V}$  versus  $\text{C}_2\text{H}_4$  evolution  $<1\ \text{V}$  an inverse relationship is discerned. Clearly, the EC ring-opening processes behind  $\text{CO}_2$  evolution occur at the expense of EC reduction. By integrating the total amounts of gases during the whole experiment even a linear negative trend appears (Fig. 5). As both types of processes result in SEI products, they likely compete to cover and passivate the carbon electrode surface. By decreasing the number of oxygenic species (such as water and carbon surface groups) present in the cell, less  $\text{CO}_2$  evolution and lower amounts of SEI products are formed  $>1\ \text{V}$ . At the same time, a higher surface area will be available for direct EC reduction,  $\text{C}_2\text{H}_4$  evolution as well as  $\text{Li}_2\text{CO}_3$  and LEDC formation. If the data is extrapolated to a

hypothetical cell in which no  $\text{CO}_2$  evolves, then about 2.5 nmol  $\text{C}_2\text{H}_4/\text{cm}^2$  would be expected. Considering the total available electrode surface area ( $\sim 350 \text{ cm}^2$ ), a total amount of 875 nmol  $\text{C}_2\text{H}_4$  would form. Assuming an equal amount of  $\text{Li}_2\text{CO}_3$  and LEDC, and an SEI density of  $1.5 \text{ g cm}^{-3}$ , then the SEI layer solely formed from EC reduction would be  $\sim 2 \text{ nm}$  thick. The resulting thickness agrees with theoretical estimations needed to passivate the electrode with these products.<sup>31–34</sup>

The final composition of the SEI will depend on the relative concentrations of competing SEI initiators (be it OR,  $\text{H}_2\text{O}$ , HF, or reduced EC) and on the available electrode surface area. The resulting products eventually cover the electrode surface, thus largely inhibiting further SEI formation. However, we demonstrate herein that SEI formation is based on a competition between several possible reaction pathways, some with the same products. Major insoluble SEI products, be it  $\text{Li}_2\text{CO}_3$  or LEDC, can form either via EC reduction (Fig. 1, reactions II and IV) or EC ring-opening (Fig. 1, reactions 4c and d). Although EC reduction reaction is expected to dominate SEI formation in a simple EC containing electrolyte under galvanostatic conditions, the concentration of EC ring-opening initiators ( $\text{H}_2\text{O}$ ,  $\text{OH}^-$ , ...) will have an influence and should be kept under control to avoid extensive EC polymerization and cell impedance increase as a result of higher electrolyte viscosity. The EC reduction reaction can be favored by, for example, adding Lewis base scavenging additives such are typically found in commercial Li-ion battery electrolytes.<sup>35</sup>

## Conclusions

Herein, the competition between EC ring-opening and EC reduction reactions during SEI formation on carbon in a model Li-ion cell is investigated with OEMS and NMR. Several findings and conclusions can be drawn from the study. First, both EC ring-opening and EC reduction reactions contribute to the SEI formation on carbon, most likely with similar in-/organic carbonate products. Second, further EC ring-opening initiators (oxygenic surface groups) were identified with reactions setting in (as determined by  $\text{CO}_2$  evolution) as early as 2.5 V vs  $\text{Li}^+/\text{Li}$ . Third, although conventionally dried under vacuum and elevated temperatures, the carbon electrodes likely continue to dry when subsequently stored in an inert environment. Larger quantities of oxygenic surface groups and other Lewis bases may negatively impact the performance of the SEI. Prolonged storage of electrodes under a reductive Ar atmosphere could potentially be beneficial to SEI performance and eventually the performance of the whole cell. Fourth, the self-propagation of EC polymerization into PEG (Fig. 1, reaction 3) after initiation by oxygenic surface groups (Fig. 1, reaction 1) was confirmed with NMR. Finally,  $\text{CO}_2$  gassing reactions can easily be misinterpreted. Commonly used Li-ion carbonate-based electrolyte solutions have a high  $\text{CO}_2$  solubility, and no  $\text{CO}_2$  leave for the cell headspace before a sufficiently high  $\text{CO}_2$  concentration in the electrolyte is reached. Additionally, the  $\text{CO}_2$  evolution and consumption reactions happen simultaneously  $< 1.5 \text{ V}$ , which further adds to the complexity of  $\text{CO}_2$  reactions in LIBs.

Being the archetypical solvent in LIBs, EC still poses questions regarding its reaction pathways and SEI formation capabilities. Minor reactions occurring even on the ppm scale (when normalized to the overall reactions in the cell) must be accounted for in order to understand and mitigate the fractional capacity and energy loss LIBs suffer over time. The present study provides further insights towards a complete understanding of the SEI, where consideration of all possible reaction pathways, not only the desired one, are highlighted.

## Acknowledgments

Knut and Alice Wallenberg (KAW) Foundation (Grant 2017.0204) and Stiftelsen för Strategisk Forskning (SSF, FFL18-0269)) are acknowledged for financial support. StandUp for Energy is acknowledged for base funding.

## ORCID

Robin Lundström  <https://orcid.org/0000-0001-9070-9264>

Neeha Gogoi  <https://orcid.org/0000-0002-0481-5544>

Xu Hou  <https://orcid.org/0000-0003-0398-2006>

Erik J. Berg  <https://orcid.org/0000-0001-5653-0383>

## References

1. European commission, *Make Transport Greener* (2021).
2. K. Xu, *Chem. Rev.*, **114**, 11503 (2014).
3. S. J. An, J. Li, C. Daniel, D. Mohanty, S. Nagpure, and D. L. Wood, *Carbon N. Y.*, **105**, 52 (2016).
4. E. Peled, *J. Electrochem. Soc.*, **126**, 2047 (1979).
5. R. Fong, U. von Sacken, and J. R. Dahn, *J. Electrochem. Soc.*, **137**, 2009 (1990).
6. E. W. C. Spotte-Smith, R. L. Kam, D. Barter, X. Xie, T. Hou, S. Dwaraknath, S. M. Blau, and K. A. Persson, *ACS Energy Lett.*, 1446 (2022).
7. D. Aurbach, Y. Ein-Eli, B. Markovsky, A. Zaban, S. Luski, Y. Carmeli, and H. Yamin, *J. Electrochem. Soc.*, **142**, 2882 (1995).
8. D. Aurbach, M. D. Levi, E. Levi, and A. Schechter, *J. Phys. Chem. B*, **101**, 2195 (1997).
9. M. Leibing, C. Peschel, F. Horsthemke, S. Wiemers-Meyer, M. Winter, and S. Nowak, *Batter. Supercaps*, **4**, 1731 (2021).
10. B. von Holtum, M. Kubot, C. Peschel, U. Rodehorst, M. Winter, S. Nowak, and S. Wiemers-Meyer, *ChemSusChem*, e202201912 (2023).
11. M. Metzger, B. Strehle, S. Solchenbach, and H. A. Gasteiger, *J. Electrochem. Soc.*, **163**, A1219 (2016).
12. L. Gireaud, S. Grugeon, S. Laruelle, S. Pilard, and J.-M. Tarascon, *J. Electrochem. Soc.*, **152**, A850 (2005).
13. M. Metzger, C. Marino, J. Sicklinger, D. Haering, and H. A. Gasteiger, *J. Electrochem. Soc.*, **162**, A1123 (2015).
14. B. D. McCloskey, A. Speidel, R. Scheffler, D. C. Miller, V. Viswanathan, J. S. Hummelshøj, J. K. Nørskov, and A. C. Luntz, *J. Phys. Chem. Lett.*, **3**, 997 (2012).
15. A. C. Luntz and B. D. McCloskey, *Chem. Rev.*, **114**, 11721 (2014).
16. K. U. Schwenke, S. Solchenbach, J. Demeaux, B. L. Lucht, and H. A. Gasteiger, *J. Electrochem. Soc.*, **166**, A2035 (2019).
17. R. Lundström and E. J. Berg, *J. Power Sources*, **485**, 229347 (2021).
18. T. Nagaoka, Y. Uchida, and K. Ogura, *Anal. Chim. Acta*, **222**, 127 (1989).
19. M. Noel and P. N. Anantharaman, *Surf. Coatings Technol.*, **28**, 161 (1986).
20. L. Fu, K. Tang, H. Oh, K. Manickam, T. Bräuniger, C. V. Chandran, A. Menzel, M. Hirscher, D. Samuelis, and J. Maier, *Nano Lett.*, **15**, 4170 (2015).
21. M. Metzger, B. Strehle, S. Solchenbach, and H. A. Gasteiger, *J. Electrochem. Soc.*, **163**, A798 (2016).
22. N. Gogoi, T. Melin, and E. J. Berg, *Adv. Mater. Interfaces*, **9**, 1 (2022).
23. M. E. Spahr, H. Buqa, W. Andreas, D. Goers, L. Hardwick, P. Novák, F. Krumeich, J. Dentzer, and C. Vix-guterl, *J. Power Sources*, **153**, 300 (2006).
24. M. E. Spahr, H. Wilhelm, T. Palladino, N. Dupont-Pavlovsky, D. Goers, F. Joho, and P. Novák, *J. Power Sources*, **121**, 543 (2003).
25. H. P. Boehm, *Carbon N. Y.*, **32**, 759 (1994).
26. Y. R. Dougassa, C. Tessier, L. El Ouatani, M. Anouti, and J. Jacquemin, *J. Chem. Thermodyn.*, **61**, 32 (2013).
27. M. Anouti et al., *J. Chem. Thermodyn.*, **50**, 71 (2012).
28. F. Single, B. Horstmann, and A. Latz, *J. Electrochem. Soc.*, **164**, E3132 (2017).
29. F. Single, B. Horstmann, and A. Latz, *Phys. Chem. Chem. Phys.*, **18**, 17810 (2016).
30. R. Bernhard, M. Metzger, and H. A. Gasteiger, *J. Electrochem. Soc.*, **162**, 1984 (2015).
31. F. A. Soto, Y. Ma, J. M. Martinez De La Hoz, J. M. Seminario, and P. B. Balbuena, *Chem. Mater.*, **27**, 7990 (2015).
32. A. Wang, S. Kadam, H. Li, S. Shi, and Y. Qi, *npj Comput. Mater.*, **4**, 15 (2018).
33. Y. X. Lin, Z. Liu, K. Leung, L. Q. Chen, P. Lu, and Y. Qi, *J. Power Sources*, **309**, 221 (2016).
34. K. Leung, F. Soto, K. Hankins, P. B. Balbuena, and K. L. Harrison, *J. Phys. Chem. C*, **120**, 6302 (2016).
35. N. Gogoi, E. Bowall, R. Lundström, N. Mozhzhukhina, G. Hernández, P. Broqvist, and E. J. Berg, *Chem. Mater.*, **34**, 3831 (2022).